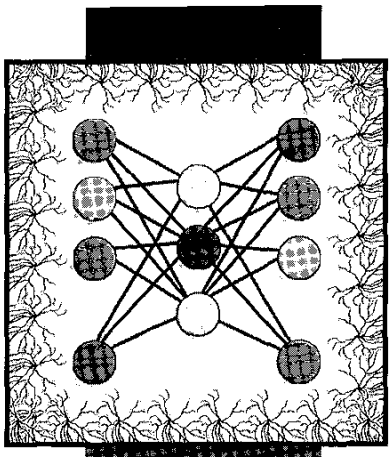

Fuzzy Neural Network-Based Texture Analysis of Ultrasonic Images

Improving Accuracy of Computer-Assisted Characterization of Diffuse Liver Diseases

S. Pavlopoulos[1], E. Kyriacou[1], D. Koutsouris[1], K. Blekas[2], A. Stafylopatis[2], P. Zoumpoulis[3]
[1]Biomedical Engineering Laboratory, [2]Computer Systems Laboratory, Department of Electrical and Computer Engineering, National Technical University of Athens
[3]Ultrasound Department, Eugenidion Hospital, University of Athens

In this article, the efficacy of a novel fuzzy neural network classifier for the characterization of ultrasonic liver images based on texture analysis techniques is investigated. Classification features are extracted with the use of image texture analysis techniques such as fractal dimension texture analysis (FDTA), spatial gray-level dependence matrices (SGLDM), gray-level difference statistics (GLDS), gray-level run-length statistics (RUNL), and first-order gray-level parameters (FOP). These features are fed to a neural network classifier based on geometrical fuzzy sets. Starting from the construction of the Voronoi diagram of the training patterns, an aggregation of Voronoi regions is performed, leading to the identification of larger regions belonging exclusively to one of the pattern classes. The resulting scheme is a constructive algorithm that defines fuzzy clusters of patterns. Based on observations concerning the grade of membership of the training patterns to the created regions, decision probabilities are computed through which the final classification is performed.

Overview

Imaging Liver Tissue with Ultrasound

Due to its ability to visualize human tissue without deleterious effects, ultrasound (u/s) B-scan imaging has become one of the most popular methods of imaging human abdominal organs such as the liver, spleen, and kidneys. The basic idea of the technique is to transmit short u/s pulses (through the human body, tissue) successively in a fan-like scanning fashion and to display the received echoes along the scan lines. Ultrasonic B-scan images appear as textured images. The pattern or speckle exhibited by biological tissues has been in routine clinical use, since the patterns for different tissues are each different. Tissue pathology, which causes change in tissue anatomical structures, may also result in a change in speckle appearance. Although the origin of these patterns is still not well understood, it is believed to be the result of a wave interference phenomenon of the echoes arriving at the transducer (scattered by structures in the tissue) and to be related to both tissue properties and the system characteristics of the imager [1].

Liver diseases can be divided into two main categories: (a) focal liver diseases, where the pathology is concentrated in a small area, while the rest of the liver volume remains normal, and (b) diffused liver diseases, where the pathology is distributed all over the liver volume. Visual interpretation of liver images by specialized physicians contributes to the decision of whether liver tissue is normal or abnormal. The decision depends on the ability of the physician to distinguish certain characteristics of the image and to compare them with those from different pathologies. Several studies have shown, however, that the characterization accuracy of diffused liver diseases using only simple visual interpretation by physicians is around 70% [2, 3].

Computer-Assisted Characterization

Computer-assisted liver tissue characterization can be defined as characterization by a physician who takes into consideration the results from a computer-based image analysis system. Computer-assisted tissue characterization has

 0739-5175/00/$10.00©2000IEEE

the advantage of providing useful information that cannot be obtained by simple visual interpretation, in addition to the fact that these techniques are less operator-dependent than traditional techniques.

The presence of various granular structures, described as texture, within liver ultrasound images makes use of image texture analysis techniques suitable for computer-assisted characterization. A considerable number of image texture analysis techniques have been developed over the years. The most common are the Laws texture energy measures (TEMs) [4, 5], the Fourier power spectrum (FPS) [5], the gray-level difference statistics (GLDS) [5, 6], the gray-level run-length statistics (RUNL) [7], the spatial gray-level dependence matrices (SGLDM) [6, 8], parameters based on first-order gray-level statistics (FOP) [9] of an image, and several techniques based on the estimation of the fractal dimension from an image such as the fractal dimension texture analysis technique (FDTA) [5]. Texture analysis techniques for liver tissue characterization have been used in the past with very promising results [5, 9, 10].

Classifying Liver Disease with Fuzzy Neural Networks

In this study, a fuzzy neural network classifier has been used for the classification of diffused liver diseases (fatty and cirrhosis from normal images) using image texture analysis data as classification features. Several models combining fuzzy systems and neural networks have been developed that build efficient pattern classifiers exploiting the particular advantages offered by each technique in a synergistic manner. Most of these methods use the training set to produce geometrical hyperboxes, and they then compute suitable membership functions in order to specify the decision boundaries of pattern classes. A popular approach to the partitioning of the input space given a set of points is based on the construction of Voronoi diagrams. A Voronoi diagram, also known as Dirichlet tessellation or Thiessen polygon, is a partition of the pattern space into convex regions. Each of these regions contains points with minimum distance from a specific point (the region generator) compared to their distance from the other points used for the construction of the diagram. Voronoi diagrams have been largely used in pattern-recognition problems because they provide a topological division of the pattern space based on the nearest neighbor property. This property has been widely exploited in pattern-recognition approaches.

The fuzzy neural approach considered here [11] creates fuzzy sets from the Voronoi diagram of the training patterns and builds class boundaries in a statistical manner. Given a set of points in the feature space, the resulting Voronoi diagram can be viewed as a puzzle, and the Voronoi regions as the pieces of this puzzle. We can assemble neighboring pieces according to their position and class, in order to specify appropriately the boundaries between classes. This formulation leads to a reduced Voronoi diagram where the new broader regions contain more than one adjoining Voronoi region having the same class label. The resulting aggregate regions are no longer convex, and they may be considered as fuzzy sets by defining membership functions indicating the degree of belongingness of points of the input space to each region. Each fuzzy set is characterized by a set of hyperplanes (separating the corresponding region from other regions) and a class label.

After constructing the fuzzy sets, decision probabilities are computed based on the density of membership values for each region and the respective performance in the selection of the correct region. Through discretization of the membership axis, a probabilistic function is created that establishes a correspondence between membership values in a specific region and the probability of correct classification. By mapping the above procedure into a neural architecture, we are able to obtain an algorithm for the design of fuzzy neural networks for pattern classification.

Methods

The analysis presented in this study was performed in two main steps: (a) the extraction of tissue characterization features, and (b) the classification of the images using a fuzzy neural network classifier.

Three sets of u/s liver images were used: normal, fatty, and cirrhotics. All abnormal cases were histologically proven. All ultrasound images were captured using an Acuson 128 XP/10 ultrasound scanner with a 3.5 MHz transducer (Acuson V328 phased array). Digital images were captured using a Fast model Screen Machine frame grabber on a PC-AT personal computer. Images were digitized with 320 × 256-pixel and 256 gray-level distribution. Texture analysis algorithms were applied in each image on a 32 × 32-pixel region of interest (ROI) selected in a systematic way so as to avoid deviation in image statistics:

i. All images were taken by the same physician, using the same equipment.

ii. Ultrasound system settings, which affect image texture, were kept the same.

iii. Fatty and cirrhosis images were histologically proven.

iv. ROI were selected by expert physicians so as to contain only liver parenchyma (normal or abnormal), with no major blood vessels. ROI were selected along the focusing area and along the center-line of each image. A representative image from each set can be seen in Fig. 1. The techniques used for feature extraction and classification are presented below.

Image Texture Analysis Techniques

Five different image texture analysis techniques were used (FOP, GLDS, RUNL, SGLDM, and FDTA) and are detailed in this section.

First-Order Gray-Level Parameters (FOP)

In this category, the parameters are derived from the gray-level histogram, and they describe the gray-level distribution without considering spatial independence. As a result, they can only describe echogenity of texture and the diffuse variation characteristics within the ROI. In our study we used Kurtosis (KUR):

$$\mathrm{KUR} = \frac{1}{N}\left[\frac{\sum_i \sum_j (g(i,j)-\mu)^4}{\sigma^4}\right] \quad (1)$$

and Variance (VAR):

$$\mathrm{VAR} = \frac{1}{N}\sum_i \sum_j (g(i,j)-\mathrm{MEA})^2 \quad (2)$$

where $g(i, j)$ is the gray level of the pixel (i, j), N is the total number of pixels in the specified ROI, and μ and σ are the mean value and standard deviation of the total number of pixels, respectively.

Gray-Level Run-Length Statistics (RUNL)

This technique is based on gray-level run length of the image. If we examine the points that lie along some given direction (run lengths), we will occasionally find runs of consecutive points that all have the

same gray level. In a coarse texture, relatively long runs occur more often, whereas fine texture contains primarily short runs. In a directional texture, the run lengths that occur along a given line should depend on the direction of the line. The feature used was Run Percentage (RP):

$$\mathrm{RP} = \frac{\sum_{i}^{N_g}\sum_{j}^{N_r} Q_{R-L}(i,j)}{P} \qquad (3)$$

where Q_{R-L} is the number of run-lengths j for gray level i, in some direction θ; N_g is the number of gray levels of the image; N_r is the number of different run lengths; and P is the total number of image pixels. Run lengths for $\theta = 0°, 45°, 90°, 135°$ and the sample mean and standard deviation were estimated.

Gray-Level Difference Statistics (GLDS)

The GLDS algorithm is based on the assumption that useful texture information can be extracted using first-order statistics of an image. The algorithm is based on the estimation of the probability density of image pixel pairs at a given distance $\delta = (\Delta_x, \Delta_y)$, having a certain absolute gray-level difference value. Coarse-texture images occur at low gray-level difference values, whereas fine-texture images result from interpixel gray-level differences with great variances. The features used are Entropy (ENT):

$$\mathrm{ENT} \equiv -\Sigma\, p_\delta(i)\log(p_\delta(i)), \qquad (4)$$

Angular Second Moment (ASM):

$$\mathrm{ASM} \equiv \Sigma p_\delta(i)^2 \qquad (5)$$

and Mean (MEA):

$$\mathrm{MEA} \equiv (1/m)\Sigma i p_\delta(i) \qquad (6)$$

where i is two pixels gray-level difference, m is the number of gray levels, and p_δ are the individual probabilities. Features were estimated for the following distances $\delta = (d,0),(d,d),(-d,d),(0,d)$.

Spatial Gray-Level Dependence Matrices (SGLDM)

The SGLDM algorithm is based on the assumption that texture properties of an image are contained in the overall or "average" spatial relationship between the gray levels. SGLDM is based on the estimation of the second-order conditional probability density $p(i, j; d, \theta)$. Each value $p(i, j; d, \theta)$ represents the probability that two different resolution cells that are on the direction specified by an angle θ and distance d will have values i and j, respectively. When texture is coarse and d is small compared to the texture elements ("speckle pattern"), then the pairs of points with distance d will have similar gray levels, so the points on the main diagonal of the matrices $p(i, j; d, \theta)$ will have large values. On the other hand, if texture is smooth, the values of the matrices will be more spread out. The features used in this algorithm are Sum Entropy (SENT):

$$\mathrm{SENT} = -\sum_{i=2}^{2N_g} p_{x+y}(i)\log\{p_{x+y}(i)\}, \qquad (7)$$

Angular Second Moment (ASM):

$$\mathrm{ASM} = \sum_i\sum_j \{p(i,j)\}^2, \qquad (8)$$

Inverse Difference Moment (IDM):

$$\mathrm{IDM} = \sum_i\sum_j \frac{1}{1+(i-j)^2}\, p(i,j), \qquad (9)$$

and Contrast (CON):

$$\mathrm{CON} = \sum_{i=1}^{N_g-1} n^2 \left\{ \sum_{i=1}^{N_g}\sum_{\substack{j=1 \\ |i-j|=k}}^{N_g} p(i,j) \right\} \qquad (10)$$

where N_g is number of gray levels, μ_x and σ_x are the mean and standard deviation of the row sums of the matrix $p(i, j)$, and μ_y and σ_y are the corresponding statistics of the column sums, with p_{x+y} and p_{x-y} given by:

$$p_{x-y}(k) = \sum_{i=1}^{N_g}\sum_{\substack{j=1 \\ |i-j|=k}}^{N_g} p(i,j), \quad k = 0,1,\ldots,N_g - 1 \qquad (11)$$

$$p_{x+y}(k) = \sum_{i=1}^{N_g}\sum_{\substack{j=1 \\ i+j=k}}^{N_g} p(i,j), \quad k = 2,3,\ldots,2N_g \qquad (12)$$

Each measure was evaluated for $d = 1$, 2, 3 and $\theta = 0°, 45°, 90°, 135°$; features were obtained from the sample mean and standard deviation of the estimated values.

Fractal Dimension Texture Analysis (FDTA)

This technique is based on the fractional Brownian motion (FBM) model developed by Madelbrot [12]. FBM, a nonstationary stochastic process, can be described by a single parameter: the fractal dimension D where $D = E + 1 - H$. The parameter H is called the Hurst coefficient, and $E + 1$ is the Euclidean dimension of the embedding space of the fractal. FBM and corresponding H and D parameters can be used to describe the roughness of different surfaces. Intensity of an ultrasonic image can be described by FBM, so fractal dimension can be used to characterize ultrasonic images. Fractal dimension D_f [3] is estimated from:

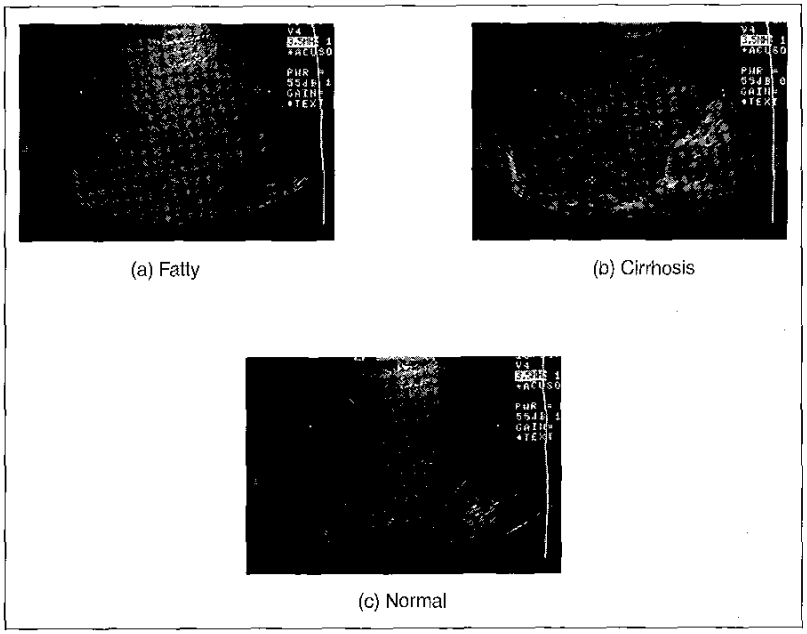

(a) Fatty (b) Cirrhosis (c) Normal

1. Ultrasonic liver images, representative from each data set. 32-by-32-pixel regions of interest systematically selected were used in the analysis.

The fuzzy neural approach creates fuzzy sets from the Voronoi diagram of the training patterns and builds class boundaries in a statistical manner.

$$E(\Delta I^2) = c(\Delta r^2)^{(6-2D_f)} \quad (13)$$

where $E(.)$ denotes the expectation operator $\Delta I = I(x_1, y_1) - I(x_2, y_2)$, $\Delta r = \|(x_2, y_2), (x_1, y_1)\|$, and c is a constant. The estimation of D_f can be done by calculating the parameter $H(D_f = E + 1 - H)$, where $E + 1$ is the Euclidean dimension and H is estimated from the equation:

$$E(|\Delta I|) = \lambda(\Delta r)H \quad (14)$$

where $\lambda = E(|\Delta I|)_{\Delta r=1}$.

Fractal-dimension texture analysis, as proposed by Wu, et al. [5], is based on computation of the Hurst coefficient of an image region for different resolution levels. Each resolution level is computed from its higher resolution level using the pyramidal approach:

$$\begin{aligned} I^{(i)}(x,y) = [\, & I^{(i+1)}(2x,2y) + I^{(i+1)} \\ & (2x+1,2y) + I^{(i+1)} \\ & (2x,2y+1) + I^{(i+1)} \\ & (2x+1,2y+1)]/4 \\ & 0 \le i < m, 0 \le x, y < 2^i \end{aligned} \quad (15)$$

[e.g., level $2^4 \times 2^4$ (16×16) is extracted from level $2^5 \times 2^5$ (32×32)] where $I^{(i)}$ represents the image intensity function on level $i(2^i \times 2^i)$. The Hurst coefficient is first computed for the original image region $2^m \times 2^m (H^{(m)})$, then for $2^{m-1} \times 2^{m-1} (H^{(m-1)})$, and so on. In our study, only the Hurst coefficients for levels 32×32 (original region) H_5, and 16×16 H_4 were used.

Fuzzy Neural Network Classifier

We used a fuzzy neural network classifier to discriminate the three classes of images. The classifier creates fuzzy sets from the Voronoi diagram of the training patterns and builds class boundaries in a statistical manner [11].

Voronoi Diagrams and Neural Networks

The Voronoi diagram or Dirichlet tessellation is a fundamental concept in computational geometry with many applications. Voronoi diagrams reveal proximity information about a set of given points in a very explicit and computationally useful manner [14].

Let $D(a,b)$ denote the Euclidean distance between two points a and b in R^d. Given a finite set $A = \{a_1, ..., a_N\}$ of points in R^d, a Voronoi region $V_n (n = 1,...,N)$ is defined as the set of points:

$$V_n = \{x \in R^d | D(x, a_n) \le D(x, a_k) \forall k \ne n\}. \quad (16)$$

Each Voronoi region V_n contains those points of R^d for which the point a_n is the closest. The partition of R^d implied by the Voronoi regions $V_1,...,V_N$ is the Voronoi diagram for the set A. Each element of A is called a *generator* of the Voronoi diagram. A common boundary of two Voronoi regions is the perpendicular bisector (hyperplane) of the segment joining the pair of respective generators. Thus, each Voronoi region is defined as the intersection of a finite number of halfspaces determined by the hyperplanes. A point at which boundaries of three or more Voronoi regions meet is called a Voronoi point.

Several algorithms for the construction of Voronoi diagrams have been proposed. Classical Voronoi diagrams can be constructed by obtaining the convex hull of the given set of points [13, 14, 15] or by incremental insertion of the Voronoi regions [16, 17, 18]. The application of Voronoi diagrams to the design of neural networks has been recently considered. In [19], two neural network construction algorithms for pattern classification are proposed that rely directly or indirectly on the Voronoi tessellation of the input space produced by the given training patterns. A systematic procedure for designing neural networks following the same principle is proposed in [20, 21]. These methods specify the architecture of the neural model based on the construction of the corresponding Voronoi diagrams for the training data. They also describe ways to specify the values of the connection weights and thresholds of each node at all layers of the neural architecture. The neural network design is robust and adaptable in order to accommodate new training patterns. It must be noted that these approaches essentially suggest ways to implement a Voronoi diagram using a neural architecture, and the classification behavior of the resulting networks is equivalent to that of nearest neighbor techniques.

In [22], an analogous construction approach was presented that incorporated the idea of fuzzy classification by defining fuzzy decision boundaries for the regions of the tessellation. This scheme was based on an approximate incremental construction of Voronoi diagrams and allowed on-line supervised learning using appropriately defined fuzzy membership functions.

Reducing the Voronoi Regions

Consider a classification problem with d continuous attributes, such that N d-dimensional patterns belong to K distinct classes. By constructing the Voronoi diagram of these generators, the d-dimensional feature space is divided into N regions reflecting the *proximity* property.

In pattern recognition, we are mostly interested in dividing the input space into a number of regions (clusters) characterized by the same class label. In general, the number of clusters is much smaller than the number of patterns. The Voronoi diagram divides the space into the same number of compartments as the input patterns, which is not very convenient. Nevertheless, if we managed to join Voronoi regions that are of the same class, we would only consider clusters of patterns. This can be achieved by removing all those hyperplanes (boundaries) of the Voronoi regions that bisect pairs of patterns (generators) belonging to the same class. In this way, the feature space is divided into regions larger than Voronoi regions, where each of these regions is associated with exactly one class label. We shall refer to these major regions as class regions, as they come from the union of neighboring Voronoi regions whose generators correspond to the same class. Figure 2 illustrates such a construction on the 2-D space for a set of 10 input points belonging to two classes (dotted lines are present in a classical Voronoi diagram).

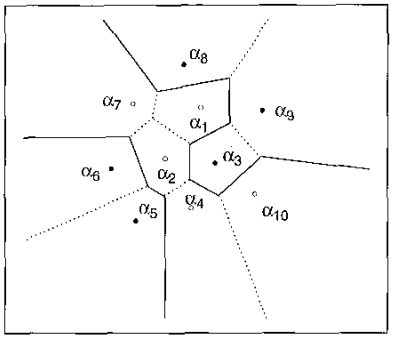

2. Schematic representation of class regions.

More specifically, we can define a class region as the union of a set of Voronoi regions, such that each region is adjoining (has common boundaries) with at least one other region of the set, and their generators belong to the same class. Each class region is characterized by a set of equations that describe the hyperplanes defining class borders. The number of new regions may be equal to or greater than the number K of classes. We only keep large class regions, since small regions containing few generators may be considered as outliers or black holes inside large clusters, and they therefore can be ignored.

In fact, the Voronoi diagram can be treated as an undirected graph, where vertices represent generators (or equivalently regions), and edges join vertices corresponding to adjoining Voronoi regions. This graph configuration is equivalent to the construction known as *Delaunay triangulation*. In order to form class regions, we start with an arbitrary Voronoi region and mark it as belonging to the first class region. Then we perform a search of the graph structure. The information available from the original construction of the Voronoi diagram is sufficient for performing the search. (Depth-first or breadth-first search could be used.) All regions connected to the starting region and bearing the same class label are marked as belonging to the same class region. Neighboring regions bearing a different class label are left unmarked, to be included in some subsequent aggregation. A similar procedure is followed from any region marked during the search. When the search is exhausted (i.e., no more Voronoi regions can be included in the current class region), a new unmarked region is selected and the procedure is repeated to construct a new class region, until there are no more unmarked Voronoi regions.

In order to encourage the formation of nearly convex class regions, we impose the following restriction during the above aggregation phase. The search can only proceed from the current Voronoi region if the number of neighboring regions bearing the same class label as the current one exceeds a given threshold value λ. If this criterion is not satisfied, the remaining neighboring regions of the current one are left unmarked (independently of their class labels), and the search is continued from some other region. The choice of the value of λ is related to the average number of boundaries of a Voronoi region, which in turn depends upon the dimension of the feature space. In our implementation, appropriate values of the parameter λ were determined experimentally for the different classification problems considered.

After construction of the reduced Voronoi diagram, it is possible to exploit proximity information for the purposes of classification. In order to formulate the problem as a fuzzy classification problem, we must give an estimation of how much a new pattern belongs to each class region, thus considering class regions as fuzzy sets. When a new input pattern $a = (a_1,...,a_d)$ is presented, an appropriate fuzzy membership value (in [0,1]) is computed. The membership function $\mu_i(a)$ for the ith class region must measure the degree to which the given pattern falls inside or outside the region. This can be considered as a measurement of how far the pattern is situated from all the hyperplanes that define the boundaries of the class region. When the pattern a is in the interior of the region and far from the hyperplanes, then the value of $\mu_i(a)$ is large, which means that the point is close to some generator having participated in the formation of that class region.

When the pattern falls outside the region, then the membership value approaches zero, which means that the point is close to some generator belonging to a different class region.

A function respecting the above guidelines is the average value of the exponential differences between the vertical distances $x_h(a)$ of the input pattern from all hyperplanes h supporting the class region I and the distances l_h of the respective generators from each hyperplane h. (Clearly, within each class region, there is a generator associated with each supporting hyperplane of the region.) It must be noted that the information concerning the distances l_h is already known from the original Voronoi diagram and is stored for each h. The vertical distance $x_h(a)$ of a pattern $a = (a_1,...,a_d)$ from a hyperplane h (described by the equation $\pi_{h1}x_1+...+\pi_{hd}x_d+\pi_{h,d+1}=0$) is computed as follows:

$$x_h(a) = \frac{\left|\sum_{j=1}^{d}\pi_{hj}a_j + \pi_{h,d+1}\right|}{\sqrt{\sum_{j=1}^{d}\pi_{hj}^2}} \tag{17}$$

Each h divides the pattern space into two halfspaces. Consider the quantities $u_{ih}(a)$, which take the values 1 or −1 depending on whether or not the generator corresponding to hyperplane h and belonging to region i is situated in the same halfspace (defined by h) as the pattern a.

The membership function of class region i can be computed as follows:

$$\mu_i(\alpha) = \frac{1}{2|H_i|}\sum_{h\in H_i} m_i^h(a) + \frac{1}{2} \tag{18}$$

where H_i is the set of hyperplanes defining class region i (having cardinality $|H_i|$) and m_i^h has the following form:

$$m_i^h(a) = \begin{cases} u_{ih}(a)\exp\left(\dfrac{-|x_h(a)-l_h|}{\sigma_1}\right) \\ \text{if } x_h(a) \le l_h \\ u_{ih}\exp\left(\dfrac{-|x_h(a)-l_h|}{\sigma^2}\right) \\ \text{if } x_h(a) > l_h \text{ and } u_{ih}(a) = 1 \\ -1 \\ \text{otherwise} \end{cases} \tag{19}$$

A graphical representation of Eq. (20) is shown in Fig. 3, which represents m_i^h as a function of the quantity $u_{ih}(a)x_h(a)$. Based on this quantity, we divide the space into three zones with respect to the hyperplane h, with each zone being characterized by different properties. In the *first zone*, the pattern is close to the hyperplane ($x_h(a) \le l_h$), independent of the side of the region border on which it is situated. Starting from the value −1 (when $x_h(a) = l_h$ and $u_{ih}(a) = -1$), the value of m_i^h increases with a steep slope until it reaches the highest value of 1 (when $x_h(a) = l_h$ and $u_{ih}(a) = 1$). The *second zone* is related to the case where the pattern and the generator are on the same halfspace, but the pattern is far from the hyperplane ($x_h(a) > l_h$ and $u_{ih}(a) = 1$). Although the pattern lies on the good side of the hyperplane with respect to the class re-

gion, we must be cautious to avoid circumstances where the pattern is at a long distance from the hyperplane and does not belong to the class region. For this reason, the value of m_i^h decreases to zero (but with a smoother slope) as the vertical distance, $x_h(a)$, from the hyperplane grows. From the above specification, it is clear that the value of σ_1 in the first zone must be higher than the value of σ_2 in the second zone to achieve the desired slope. The *third zone* represents the case where the pattern is situated far outside the region of interest and far from the hyperplane h ($x_h(a) > l_h$ and $u_{ih}(a) = -1$). In this case, m_i^h takes its lowest value, -1.

It must be noted here that $m_i^h(a)$ does not include precise information about whether or not the pattern is situated inside the class region. Even when the pattern and the generator are in the same halfspace with respect to the hyperplane, we are not aware of what happens with other hyperplanes, as we individually examine each hyperplane and not the whole region. After computing all the $m_i^h(a)$ values, we obtain a global estimation of the degree of belongingness of pattern a to the region i through the value of the membership $\mu_i(a)$.

The above membership function takes into account useful proximity information provided by the characteristics of the original Voronoi construction, such as the equations describing hyperplanes, the position of generators relative to hyperplanes, and the vertical distances l_h. In addition, it exploits information related to class regions, such as the hyperplanes defining the boundaries of each class region.

Computing Decision Probabilities

In the previous sections, we have described the first phase of the proposed approach to pattern classification that incorporates the construction of the Voronoi diagram corresponding to the training patterns, the integration of Voronoi regions to a number of class regions, and the definition of appropriate membership functions. With this kind of preprocessing, the problem of selecting the correct class is transformed to the problem of selecting the correct region. In this section, we describe how the membership values of the training patterns are used to construct models providing decision probabilities that a pattern with a given membership value can be assigned to a specific region.

After having computed the membership values corresponding to an input pattern, we could perform the classification procedure simply by selecting the class of the region with the maximum membership value. This is what happens in most fuzzy approaches to pattern classification (e.g., in the fuzzy min-max network). Unfortunately, this decision scheme does not seem to provide good classification results, since some regions tend to exhibit constantly higher membership values compared to other regions. It seems more effective to evaluate the membership of a given pattern to a region by taking into account the distribution of membership values of the training patterns to this region. This leads to the construction of a probability model for each class region, which provides useful information for the selection of the appropriate region during classification.

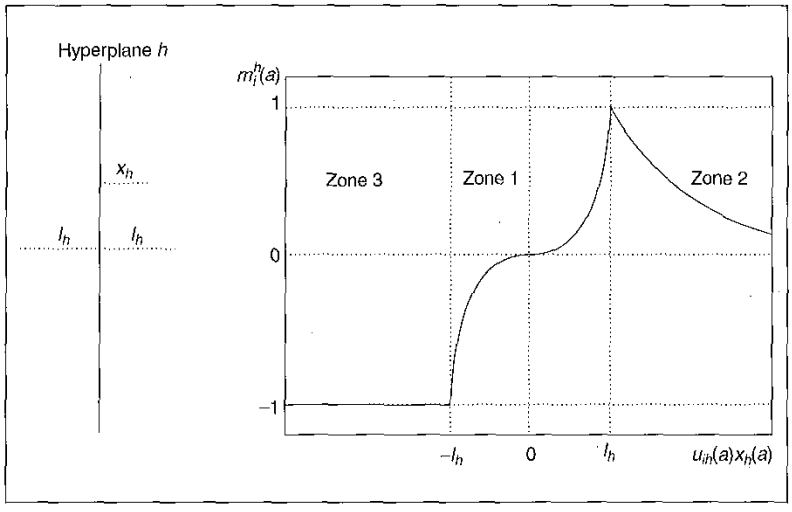

3. Fuzzy decision boundaries.

The construction of the probability models is based on the search for ranges of membership values that have more chance to lead to the successful selection of a region. More specifically, considering class region i, the interval [0,1] of membership values is divided into a number L_i of equal-size cells. To each cell v (v=1, ..., L_i), we assign a probability value p_i^v computed as the percentage of the training patterns belonging to region i that have their membership value in the cell v.

It should be observed that, after the membership values of training patterns to each region have been computed, it is possible to view the classification problem as mapping from the space of membership vectors to the set of classes, $c:(\mu_1,...,\mu_R) \rightarrow \{1, ..., K\}$ (where R is the number of class regions and K is the number of classes). Such a mapping can be easily constructed using, for example, a multilayer perceptron trained by the backpropagation algorithm or any of its variants. Although this approach is intuitively more appealing and exhibited excellent performance on training sets, its performance on the test set was inferior (in all examined datasets) compared with the approach based on the probability model.

Neural Network Implementation

In the previous paragraphs, we have shown how one can construct fuzzy sets (corresponding to class regions) starting from a Voronoi diagram, as well as how a model of probabilities can be built for each fuzzy set using the distribution of membership values. The proposed construction algorithm can be summarized into the following steps:

1. Construct the classical Voronoi diagram of a set of N patterns
2. $A = \{a_1,...,a_N\}$, in a d-dimensional space.
3. Reduce the Voronoi diagram into a number of class regions.
4. Discard small class regions and let R be the number of the remaining large class regions.
5. For each pattern a_j, $j = 1,...,N$, compute the membership values $\mu_i(a_j)$, $i = 1, ..., R$.
6. For each region i, $i = 1, ..., R$, categorize the membership values in a histogram using a number L_i of equal-size cells in [0,1].
7. Compute selection probabilities p_v^i, $i = 1,...,R$, $v = 1,...,L_i$.

In order to use the method for the classification of a new pattern, the member-

ship values of the pattern to each region i are first computed. Then, the corresponding probabilities p_i^v are determined (where v represents the cell containing the membership value of the pattern) and the region i with maximum p_i^v is selected. The class of this region is considered as the final classification decision.

The above decision approach can be implemented by means of a neural network architecture, as illustrated in Fig. 4. The architecture consists of five layers, and connections exist only between successive layers. The first layer is the input layer, having as many nodes as the dimension of patterns. The nodes in the second layer represent hyperplanes that define class regions. For each class region i there are $|H_i|$ nodes, one for each hyperplane supporting that class. As a hyperplane separates two regions, there will generally be two nodes referring to the same hyperplane (except for hyperplanes supporting small regions that were discarded during construction). Each second-layer node computes the value of the function m_i^h for an input pattern using Eq. (19).

The third layer contains as many nodes as the number R of class regions. The output of each node i of this layer provides the membership value μ_i of the pattern to the corresponding region, as computed in Eq. (18). The connections between nodes of the second and third layers assume binary values 1 or 0 to associate regions with their supporting hyperplanes.

The fourth layer implements the membership histogram. Each region i of the third layer is connected to L_i nodes of the fourth layer, corresponding to the cells of the histogram. Each such node v ($v = 1, ..., L_i$) fires only in the case where the μ_i value falls inside the corresponding cell and provides the respective probability p_i^v; otherwise, the output of the node is zero. This representation allows an efficient implementation of the histogram by means of simple nodes yielding a fixed output on an on-off basis.

The fifth layer embodies one node for each of the K classes. If region i has class label k, then the set of I_i nodes of the fourth layer (representing the histogram of region i) is connected to node k of the fourth layer. In other words, the connections between nodes of the fourth and fifth layers take binary values 1 or 0 to associate class regions (histogram cells) with class labels. The output ξ_k of each node k of the last layer is taken equal to the maximum of the outputs (probabilities p_i^v) of the cell nodes connected to that node. Finally, the class k with the maximum ξ_k is the decision of the fuzzy neural classification network.

When a new pattern a is applied to the network, the membership values $\mu_i(a)$ of the pattern to each class region i are initially computed. The computation proceeds by determining the probabilities p_i^v corresponding to the respective histogram cells. The decision of the network is the class of the region with the maximum probability p_i^v expressed by the quantity ξ_k. As is the case with other neural network designs based on Voronoi diagram information [20-22], the method has the ability to define completely the neural structure, namely the number of hidden layers and nodes of each layer, along with the connection values between nodes of successive layers. The proposed neural architecture incorporates an additional layer with respect to other approaches, accounting for the computation of decision probabilities.

Results

To evaluate the performance of the proposed computer-assisted tissue-characterization algorithm, we used a total of 150 images (normal, fatty, and cirrhotic). In the first phase, the 12 texture analysis features described above were calculated for all the images. Also as described above, 32-by-32-pixel ROI were selected in each image, and the corresponding texture features were calculated. These features have been shown to contain useful information for characterizing liver tissue pathology [10].

The second phase consisted of using the proposed fuzzy neural network classifier to discriminate liver abnormalities. For this task, a set of 75 images (25 from each class) was used as the learning set for the classifier, whereas another 75 images (25 from each class) were used as a test set. The performance of the classifier was then evaluated using different combination of classification features (image texture analysis features). Due to the large number of different subset combinations, only those that resulted in a correct classification accuracy rate of greater than 75% are presented in this study. To reduce the computational complexity in the training and classification process, we decided to limit the number of features used in the classification down to six. In that sense, combinations of six or less features (out of the 12 presented previously) were used for the classifications. Table 1 shows the

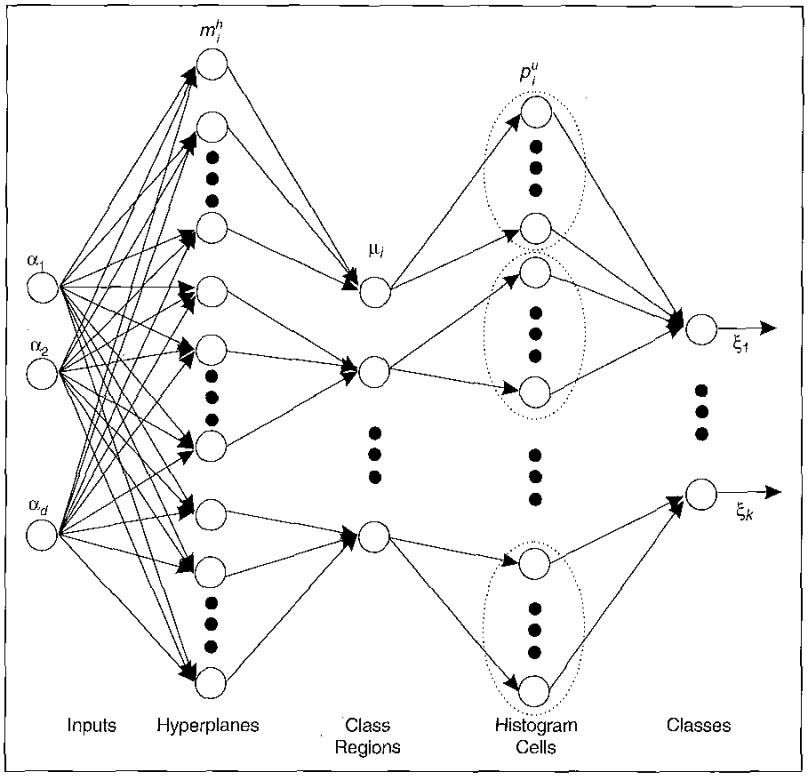

4. Proposed neural network architecture.

Table 1. Correct classification rates for the fuzzy neural network classifier.

Feature Set (Features Presented in Text)	Normal	Fatty	Cirrhosis	Total
FOP_KUR, GLD_ASM, GLD_MEA, SGLD_ASM, SGLD_IDM, RUNL_RP	80.00%	88.00%	80.00%	82.67%
GLD_ENT, SGLD_SENT, SGLD_CON, RUNL_SRE, FDTA_H4, FDTA_H5	76.00%	84.00%	80.00%	80.00%
FOP_KUR, GLD_ASM, SGLD_SENT, SGLD_IDM, RUNL_RP, FDTA_H4	80.00%	80.00%	76.00%	78.67%
FOP_KUR, GLD_ASM, GLD_MEA, SGLD_ASM, RUNL_RP	76.00%	84.00%	68.00%	76.00%

results of the proposed classifier in discriminating the different pathologies.

It is apparent that the proposed classifier provides high classification accuracy for all different pathologies. In particular, the *<KYR, ASM, MEA, ASM, IDM, RP>* set achieves an overall 82.67% accuracy in characterizing the different pathologies, whereas individual accuracy is 80.00%, 88.00%, and 80.00% for normal, fatty, and cirrhotic liver, respectively. Similar (although somehow lower) accuracy is obtained with two more feature sets of size six (accuracies of 80.00% and 78.67%, respectively). All these figures are higher than those achieved by visual inspection by physicians (approximately 70% for diffuse liver diseases [4, 5]). Furthermore, in all cases the proposed fuzzy neural network classifier achieved higher accuracy than a conventional 1-nearest-neighbor or K-NN classifier).

In addition, the classification experiment verified the usefulness of the proposed image texture analysis features in discriminating liver tissue pathology in ultrasound images. Even subsets of texture features of size five (see Table 1) were able to discriminate the different pathologies with accuracy higher than the 75% accuracy limit that we have set for the experiment. However, the reduced classification accuracy achieved with less than six features indicates that useful information is lost when a smaller feature set is used for classification. Due to the fact that the number of image texture features that were used in this experiment is only part of the image texture features available, we can easily understand the possibilities the proposed methodology offers in computer-assisted diffuse liver disease characterization.

Conclusions

Computer-assisted characterization of ultrasonic liver images using image texture analysis techniques and fuzzy classifiers has been tested and evaluated. In particular, we have implemented a neural network classifier that is based on geometrical fuzzy sets. The approach is based on the construction of Voronoi diagrams in the pattern space and the creation of region aggregates inside the Voronoi puzzle. For the constructed class regions, decision probabilities are computed in terms of the distribution of membership values to these regions. The whole technique can be implemented by means of a five-layer feedforward neural network architecture.

Experimental results indicate that the proposed method is effective in terms of the rate of correct classification and that it has the ability to overcome the difficulties arising from the problem of overlapping classes. Moreover, it has the characteristic of maintaining the powerful geometrical features of the Voronoi structure, as well as of creating efficient decision boundaries through the statistical processing of membership values. This work allows us to experiment further with the use of proximity-based approaches to the construction of fuzzy neural classifiers, and to discover more efficient techniques in the area of soft decision making. Since the complexity of the construction of Voronoi diagrams becomes high as the dimension of the feature space grows, we are interested in applying effective geometrical algorithms that can suggest neighbors of a given pattern (in the sense of the Voronoi diagram) for large dimensional problems.

Furthermore, the results of this work have demonstrated the ability of using image texture analysis techniques to extract features that characterize liver tissue abnormalities. The proposed features, when combined in a feature set of size six, achieved a higher classification accuracy for diffuse pathologies than that reported for physicians and than those obtained by nearest neighbor classification. Furthermore, the fact that a feature set of size six obtained higher accuracy than all subsets of features of size five or less indicates that the feature is complementary in characterizing the pathologies involved.

In conclusion, we should point out that an ultrasonic image depends on many factors, and characterizing ultrasonic images is not a trivial task. Initial results proved to be very promising. Furthermore, we expect that further evaluation of the techniques using larger image data sets and the incorporation of additional algorithms will improve the overall accuracy of the method.

Sotiris Pavlopoulos was born in Athens, Greece, in 1965. He received his degree in electrical engineering from the University of Patras, Greece, in 1987 and his M.Sc. and Ph.D. in biomedical engineering in 1990 and 1992, respectively, from Rutgers University, New Brunswick. From 1992 to 1995, he was a postdoctoral fellow at the National Technical University of Athens. He is currently a research assistant professor at the Institute of Communication and Computer Systems of the National Technical University of Athens. His current research interests include medical informatics, telemedicine, medical imaging and signal processing, and Monte Carlo simulation techniques in tomography. Dr. Pavlopoulos has been ac-

tive in a number of European R&D programs in the field of telematics applications in healthcare and as principal investigator in several European and national research programs.

Efthyvoulos K. Kyriacou was born in Paphos Cyprus in 1972. He received his diploma in electrical & computer engineering from the National Technical University of Athens (NTUA) in 1996. He is currently pursuing his Ph.D. in the Department of Electrical & Computer Engineering-NTUA in telemedicine. He has been with the Institute of Communication and Computer Systems - NTUA since 1996 as a research postgraduate student, working in the area of biomedical engineering in several EC research projects (AMBULANCE, MOMEDA, EMERGENCY-112) concerning medical informatics, medical imaging, and telemedicine. He is a student member of IEEE EMBS, IEEE Computer Society, and the Hellenic Society of Biomedical Engineering.

Dimitris Koutsouris was born in Serres, Greece, in 1955. He received the electrical engineering degree in 1978 in Greece, the DEA degree in biomechanics in 1979 in France, the Ph.D. degree in genie biologie medicale in France, and the Doctoral d'Etat in biomedical engineering in France. He has been with the University of Southern California, Los Angeles, and the Rene Descartes, Paris, France. He is currently a professor of biomedical engineering and chairman in the Department of Electrical and Computer Engineering, National Technical University of Athens, Greece. He has published over 100 research articles and book chapters and more than 150 conference communications. Dr. Koutsouris is a member of many honorary and professional societies and is currently the president of the Greek Society of Biomedical Technology.

Konstantinos Blekas was born in Karditsa, Greece, in 1969. He received the Diploma degree in electrical and computer engineering in 1993, and the Ph.D. degree in computer science in 1997, both from the National Technical University of Athens. His research interests include neural networks, hybrid systems, and intelligent diagnostic techniques. Dr. Blekas is a member of the IEEE Computer Society and the Association for Computing Machinery.

Andreas-Georgios Stafylopatis was born in Athens, Greece, in 1956. He received the Diploma degree in electrical and electronics engineering in 1979 from the National Technical University of Athens, and the Docteur Ingenieur degree in computer science in 1982 from the University of Paris-Sud, Orsay, France. Since 1984, he has been with the Department of Electrical and Computer Engineering, National Technical University of Athens, where he is currently a professor. His research interests include parallel processing and computational intelligence. Dr. Stafylopatis is a member of the IEEE Computer Society; the IEEE Systems, Man, and Cybernetics Society; the Association for Computing Machinery; the European Neural Network Society; and the International Neural Network Society.

Paul Zoumpoulis was born in Athens, Greece, in 1953. He received his Diploma from the Medical School of Athens University (MD) in 1976. He is currently medical director of the Ultrasound Department of the 251 Military Aviation Hospital, and he is chief medical director of the Ultrasound Department of the Eugenideio University Hospital in Athens, Greece.

Address for Correspondence: Dr. Sotiris Pavlopoulos, Biomedical Engineering Laboratory, Department of Electrical and Computer Engineering, National Technical University of Athens, 9 Iroon Polytechniou St., GR-157 73 Zografou, Athens, Greece. Tel: +30-1-7722429. Fax: +30-1-7722431. E-mail: spav@biomed.ntua.gr.

References

1. **Shung Kirk K, Thieme GA:** *Ultrasonic Scattering in Biological Tissues.* Florida: CRC Press, 1993.

2. **Gosnik BB, Lemon SK, Scheible W, G. R. Leupold GR:** Accuracy of ultrasonography in diagnosis of hepatocellular disease. *AJR* 133: 19-23, 1979.

3. **Foster K, Dewbury KC, Griffith AH, Wright AHR:** The accuracy of ultrasound in the detection of fatty infiltration of the liver. *Br J Radiol* 53: 440-442, 1980.

4. **Laws KI:** Texture energy measures. *Proc Image Understanding Workshop*, pp. 47-51, 1979.

5. **Wu CM, Chen YC, Hsieh KS:** Texture features for classification of ultrasonic liver images. *IEEE Trans Med Imaging* 11: 141-152, 1992.

6. **Wenska JS, Dryer CR, Rosenfeld A:** A comparative study of texture measures for terrain classification. *IEEE Trans Syst, Man, Cybern* SMC-6: 269-285, 1976.

7. **Galloway MM:** Texture classification using gray level run lengths. *Computer Graphics and Image Processing* 4: 172-179, June 1975.

8. **Haralick RM, Shanmugan K, and Dinstein IH:** Texture features for image classification. *IEEE Trans Syst, Man, Cybern* SMC-3: 610-621, 1973.

9. **Kadah YM, Farag AA, Zurada JM, Badawi AM, and Youssef Abou-Bakr M:** Classification algorithms for quantitative tissue characterization of diffuse liver disease from ultrasound images. *IEEE Trans Med Image* 15(4), August 1996.

10. **Konnis G, Pavlopoulos S, Kyriacou E, Koutsouris D, Zoumpoulis P, Theotokas I:** Quantitative characterization of US liver images by using texture analysis techniques. *Proc RSNA 1996*, Chicago, IL, USA, December 1996.

11. **Blekas K, Likas A and Stafylopatis A:** A fuzzy neural network approach to classification based on proximity characteristics of patterns. *Proc 9th IEEE Inter Conf. on Tools with Artificial Intelligence (ICTAI'97)*, Newport Beach, CA, pp. 323-330, 1997.

12. **Mandelbrot BB:** *The Fractal Geometry of Nature.* San Francisco, CA: Freeman, 1982.

13. **Aurenhammer F:** Voronoi diagrams - A Survey of a fundamental geometric data structure. *ACM Computing Surveys*, 3: 345-405, 1991.

14. **Barber CB, Dobkin DP, Huhdanpaa H:** The Quickhull algorithm for convex hulls. *ACM Trans Math Softw* 22: 469-483, 1996.

15. **Preparata FP and Shamos MI:** *Computational Geometry - An Introduction.* New York: Springer-Verlag, 1985.

16. **Bowyer A:** Computing Dirichlet Tesselations. *The Computer Journal* 24: 162-166, 1981.

17. **Green PJ, Sibson R:** Computing Dirichlet tesselations in the plane. *The Computer Journal* 4: 778-787, 1978.

18. **Guibas L, Knuth DE, Sharir M:** Randomized incremental construction of Delaunay and Voronoi diagrams. *Algorithmica* 9: 534-560, 1992.

19. **Murphy DJ:** "Nearest neighbor pattern classification perceptrons. *Proc IEEE* 78: 1595-1598, 1990.

20. **Bose NK, Garga AK:** Neural network design using Voronoi diagrams. *IEEE Trans Neural Networks* 4: 778-787, 1993.

21. **Garga AK, Bose NK:** A neural network approach to the construction of Delaunay tesselation of poinds in R^d. *IEEE Trans Circuits and Systems - I* 41: 611-613, 1994.

22. **Blekas K, Likas A, Stafylopatis A:** A fuzzy neural network approach based on Dirichlet tesselations for nearest neighbor classification of patterns. *Proc IEEE Workshop on Neural Networks for Signal Processing (NNSP '95)*, Boston, MA, pp. 153-161, 1995.